J Solid State Eletrochem (2004) 8: 127–137
DOI 10.1007/s10008-003-0443-3

ORIGINAL PAPER

Antonio Doménech-Carbó · Francisco José Torres
Javier Alarcón

Electrochemical characterization of cobalt cordierites attached to paraffin-impregnated graphite electrodes

Received: 14 April 2003 / Accepted: 4 August 2003 / Published online: 14 October 2003
© Springer-Verlag 2003

Abstract The electrochemistry of α, β and μ cobalt-containing cordierites ($Co_2Al_4Si_5O_{18}$) attached to paraffin-impregnated graphite electrodes has been studied by linear scan and cyclic voltammetries in HCl + NaCl and NaOH electrolytes. This electrochemistry is compared with that of vitreous cobalt cordierite, cobalt(II) oxide and cobalt spinel aluminate ($CoAl_2O_4$), the two last taken as reference materials. Electrochemical processes involve the site-characteristic reduction of Co(II) species to cobalt metal near to −0.5 V vs. SCE and their oxidative dissolution near +0.3 V, accompanied by solid state interconversion between Co(II) and Co(III) at potentials above +0.45 V. Cordierite-modified electrodes display a significant site-dependent catalytic effect on the electrochemical oxidation of mannitol in 0.10 M NaOH.

Keywords Cobalt · Cordierites · Mannitol · Voltammetry

Introduction

Cordierite-based glass ceramics have claimed attention because of their low dielectric constant, high electrical resistivity and low thermal expansion. These properties allow such materials to be used for structural electronic applications [1, 2].

Magnesium cordierite ($Mg_2Al_4Si_5O_{18}$) exists in three forms: a hexagonal high-temperature form, named α-cordierite or indialite, an orthorhombic low-temperature form, labelled β-cordierite, and a metastable form, designated μ-cordierite, which can be described as a solid solution with a μ-quartz structure [3, 4].

Both α and β magnesium and cobalt cordierites are characterized by six-membered rings of tetrahedrally coordinated cations (T_2) linked through tetrahedral (T_1) and octahedral polyhedra. Alternate layers of the hexagonal rings are connected through M^{2+} octahedra and T_1 tetrahedra. Aluminium occupies mostly T_1 tetrahedra, silicon occupies T_2 tetrahedra and magnesium occupies octahedral sites. Differences between high- and low-temperature cordierites lie in a greater or lesser degree of disorder between the aluminium and silicon atoms within the T_1 and T_2 sites [5, 6]. In the case of α-cordierite, aluminium-rich tetrahedra do not occupy definite positions, whereas in β-cordierite the aluminium-containing tetahedra are placed in fixed sites.

Most natural cordierites contain other cations or molecules which either substitute for magnesium, silicon or aluminium or are inserted in the channels of the cordierite framework [7, 8]. Attempts to model the electrical, mechanical and thermal properties of cordierite solid solutions containing several dopants in the cordierite structure have been reported [9, 10, 11]. The unique case of complete metal substitution occurs with cobalt in the solid solution $Mg_xCo_{2-x}Al_4Si_5O_{18}$ ($0 < x < 2$) [12]. In prior work the monophasic cobalt-containing cordierite has been synthesized by crystallization of glasses of stoichiometric composition $2MO.2Al_2O_3.5SiO_2$ (M = Mg, Co) at various temperatures and times. The crystallization sequence and microstructural evolution was analyzed by X-ray diffraction (XRD) and field emission scanning electron microscopy (FESEM). The first crystalline phase displays the μ-cordierite structure being further converted, upon thermal treatment, into α-cordierite and β-cordierite, successively [13, 14]. IR and UV-Vis diffuse reflectance spectra suggest that the Co^{2+} ions, which occupied tetrahedral sites in the glasses, move into octahedral sites during crystallization [14, 15]. Formation of β-cordierite from α-cordierite can be considered

A. Doménech-Carbó (✉)
Departament de Química Analítica, Universitat de València,
Dr. Moliner 50, 46100 Burjassot (València), Spain
E-mail: antonio.domenech@uv.es

F. J. Torres · J. Alarcón
Departament de Química Inorgànica, Universitat de València,
Dr. Moliner 50, 46100 Burjassot (València), Spain

as an example of a transition from a relatively disordered system to an ordered one [15].

In order to gain information about these possible structural features, the voltammetry of microparticles can be used. In recent years, considerable effort has been invested in devising chemically modified electrodes for characterizing solid materials [16]. From voltammetric studies of Lamache and Bauer [17] and Brainina and Vidrevich [18] on modified carbon paste electrodes, the so-called solid state electrochemistry has been increasingly investigated. From the development of the abrasive voltammetry by Scholz et al. [19, 20], based on the transference by abrasion of traces of solid samples onto the surface of paraffin-impregnated graphite electrodes, the voltammetry of microparticles has experienced a considerable growing interest [16, 21, 22, 23].

This methodology provides information on the composition of solid phases through different electrochemical processes involving non-conducting microparticles attached to an inert electrode. The best studied electrode processes consist of oxidative dissolution of metals and alloys, reductive dissolution and oxidative dissolution of metal oxides, reductive conversion of oxides and salts to metal deposits and dissolved anions, and topotactic solid state transformations accompanied by the ingress/issue of ions from/to the adjacent solution [16]. Accordingly, it is conceivable that the voltammetry of microparticles might provide structural information concerning natural and synthetic materials (1) by characterizing the electrochemical response of structurally different materials, and (2) by detecting the coexistence of electroactive centers with different structural arrangements in a given material.

The purpose of the current work is to describe the voltammetric response of cobalt centres in synthetic α-, β- and μ-cordierites, $Co_2Al_4Si_5O_{18}$, as well as that of cobalt cordierite glass upon abrasive attachment to paraffin-impregnated graphite electrodes (PIGEs). This electrochemistry has been compared with that of $Co(NO_3)_2.6H_2O$ in solution, and those of cobalt metal and cobalt(II) oxide, in which Co^{2+} ions present an octahedral coordination, and "cobalt blue", $CoAl_2O_4$, which possess a "normal" spinel structure, the Co^{2+} centres exhibiting a tetrahedral coordination. Attention is focused on possible reduction of Co(II) centres to cobalt metal and Co(III)/Co(II) solid state interconversions. In this context, Rao et al. [24] and Frangini et al. [25] have recently studied the voltammetry of solid $LiCoO_2$, a material potentially interesting as a cathode material in lithium ion secondary batteries [26].

Cyclic and linear scan voltammetries (CV and LSV, respectively) have been used systematically upon immersion of cordierite-modified electrodes in HCl + NaCl, HCl + $MgCl_2$ and NaOH aqueous electrolytes. Semi-derivative convolution was used to improve peak resolution.

Additionally, the catalytic effect exerted by cordierite-modified electrodes on the electrochemical oxidation of mannitol in alkaline media has been investigated in order to assess the existence of a possible site-characteristic electrocatalytic effect. It is known that the catalytic effect of electrode modifiers on the electrochemical oxidation or reduction of selected analytes can enhance significantly the sensitivity and selectivity in their determination. Among others, electrode modification methods include formation of inorganic coatings on inert electrodes, whose analytical applications have been recently reviewed by Cox et al. [27]. Thus, coatings of clays [28], zeolites [29] and transition metal oxides and hydroxides [30] have been used as effective oxidizing agents for promoting the oxidation of polyalcohols, which are scarcely electroactive substrates. In this context, there has been previously reported the use of vanadium-doped zirconias attached to graphite electrodes as electrochemical sensors for determining hydrogen peroxide [31]. Such systems exhibit a remarkable site selectivity, the electrocatalytic effect being associated with seven-coordinated vanadium centres in monoclinic zirconias, but being almost entirely absent in tetragonal zirconias in which eight-coordinated sites exist.

Coatings of transition metal oxides and hydroxides have been used as effective oxidizing agents in metal-based surface-modified glassy carbon electrodes for the amperometric sensing of sugars and alditols [30, 32, 33, 34, 35, 36]. It seems that dispersed catalytic sites provide a greater electrocatalytic efficiency compared to bulk metal electrodes [30]. In view of the efficient electrocatalytic activity exerted by cobalt oxide-based glassy carbon electrodes on the oxidation of sugars and alditols, reported by Cataldi and co-workers [30, 36], the catalytic effect of cobalt cordierites on the oxidation of mannitol (taken as a model compound) has been studied in alkaline media.

Experimental

Preparation of samples

Glass precursors with stoichiometry $Co_2Al_4Si_5O_{18}$ were prepared by a semiwet method as reported elsewhere [14, 15]. Appropriate amounts of $Al(NO_3)_3.9H_2O$ and $Co(NO_3)_2.6H_2O$ were dissolved in doubly distilled water at 80 °C with vigorous stirring, then the required amounts of colloidal SiO_2 and $MgCO_3$ were added. The resulting dispersion was heated until dryness and then dried in an oven at 110 °C for 1 day. The powder was ground and calcined at 1000 °C for 2 h to remove nitrate and after regrinding the powder was melted in an alumina crucible at around 1600 °C for 3 h. The glasses were remelted twice for increasing the homogeneity and the last melt was poured into water to form a frit. After grinding the glass samples to powder with sizes < 30 μm, cylindrical pellets of powder glass were obtained by pressing at 0.5 MPa, which were subsequently calcined in an electric furnace from 700 to 1400 °C. On annealing the glass powder pellets at 800 °C for 16 h, the glass transformed to the μ crystalline form of cordierite. Specimens containing α- or β-cordierite as a unique phase were prepared by annealing the glass pellets at 1000 °C for 27 h or 1050 °C for 190 h, respectively. The prepared specimens were characterized by XRD and IR spectroscopy. The obtained results confirmed that each of the three prepared specimens were monophasic materials containing only one of the three crystalline forms of cordierite, μ, α or β.

Materials

$MgCO_3$ (Panreac), Al_2O_3 (Aldrich), colloidal SiO_2 (Degussa), $Al(NO_3)_3.9H_2O$ (Aldrich) and $Co(NO_3)_2.6H_2O$ (Aldrich) were used for sample preparation. Co powder (Fluka), CoO (Fluka) and $CoAl_2O_4$ ("cobalt blue", Kremer) were used as reference materials in the electrochemical experiments. HCl, NaCl, $MgCl_2$ and NaOH (all supplied by Panreac) were used as supporting electrolytes in dissolutions in doubly distilled water with concentrations ranging from 0.10 to 1.0 M. D-(−)-Mannitol (Merck) was used for the electrocatalytic experiments. XRD data for CoO and $CoAl_2O_4$ indicated that no significant traces of other crystalline forms existed in such materials.

Modified electrode preparation

A spectral graphite rod impregnated by paraffin in the vacuum of a water jet pump was used as the working electrode; for preparation details, see [19, 20]. The sample (0.1–1 mg) was powdered in an agate mortar and pestle and placed on a glazed porcelain tile, forming a spot of finely distributed material. Then the lower end of the PIGE was gently rubbed over that spot of the sample until all the powdered sample was transferred to the electrode surface. The electrode surface was then pressed against a dry tissue paper to remove ill-adhered particles. Complementary experiments were performed by pressing the graphite electrode against a spot of the powdered material deposited on a glass tile.

Instrumentation and procedures

Characterization of the samples was carried out by differential thermal analysis (DTA), powder X-ray diffraction (XRD), field emission scanning electron microscopy (FESEM), infrared (IR) and UV-Vis diffuse reflectance spectroscopies using the equipment previously described [14, 15].

Electrochemical experiments were performed at 298 K in a three-electrode cell under an argon atmosphere. Linear scan and cyclic voltammograms (LSVs and CVs, respectively) were obtained with BAS CV 50W equipment. In LSVs the potential was scanned either in the positive or in the negative direction without a previous electrogeneration step. Sample-modified PIGEs were dipped into the electrochemical cell so that only the lower end of the electrode was in contact with the electrolyte solution. This procedure provides an almost constant electrode area and reproducible background currents. A saturated calomel reference electrode (SCE) and a platinum wire auxiliary electrode completed the conventional three-electrode arrangement.

Results and discussion

General voltammetric response

Figure 1 illustrates the cyclic voltammetric response of PIGEs modified by (a) cobalt(II) oxide, (b) cobalt cordierite glass and (c) cobalt(II) spinel immersed in 0.10 M HCl + 0.90 M NaCl. Although a relatively similar pattern was obtained, some significant differences can be observed for such materials. Thus, for CoO an oxidation peak near to +0.75 V appears, followed by a cathodic wave at +0.55 V. At more negative potentials a cathodic wave appears around −0.50 V, followed by a prominent rising background current and an anodic peak near −0.18 V. In contrast, for cordierites, a well-defined reduction peak appears at −0.45 V, whereas in

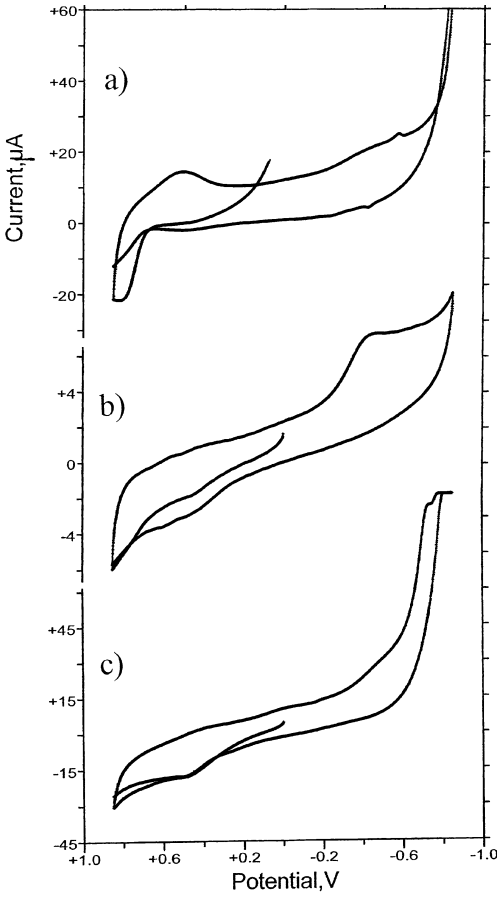

Fig. 1 CVs of PIGEs modified by (**a**) cobalt(II) oxide, (**b**) cobalt cordierite glass and (**c**) cobalt(II) spinel immersed in 0.10 M HCl + 0.90 M NaCl. Potential scan rate: 50 mV/s

the positive region of potentials, overlapped peaks are recorded between +0.40 and +0.60 V accompanied by weak cathodic signals in the same region of potentials. For cobalt(II) spinel, only one anodic peak near to +0.45 V appears in the initial anodic scan voltammograms, whereas in the cathodic scan a prominent reduction process at −0.70 V is preceded by a shoulder ca. −0.50 V.

On first examination, this electrochemistry can be described following the scheme developed by Scholz and Meyer [16] for lead oxides. Thus, for cobalt oxide the cathodic process recorded in the −0.3/−0.8 potential region can be represented as:

$$CoO(s) + 2H^+ + 2e^- \rightarrow Co(s) + H_2O \quad (1)$$

where (s) denotes solid phases. The electrochemical mechanism involves dissolution/crystallization and/or a solid-state reaction scheme [16].

In the subsequent anodic scan, the stripping oxidation of Co previously deposited appears at −0.18 V:

$$Co(s) + xCl^- \rightarrow CoCl_x^{(2-x)+} + 2e^- \quad (2)$$

On comparing the voltammetric responses of Co and CoO powders and that of $Co(NO_3)_2.6H_2O$ in solution

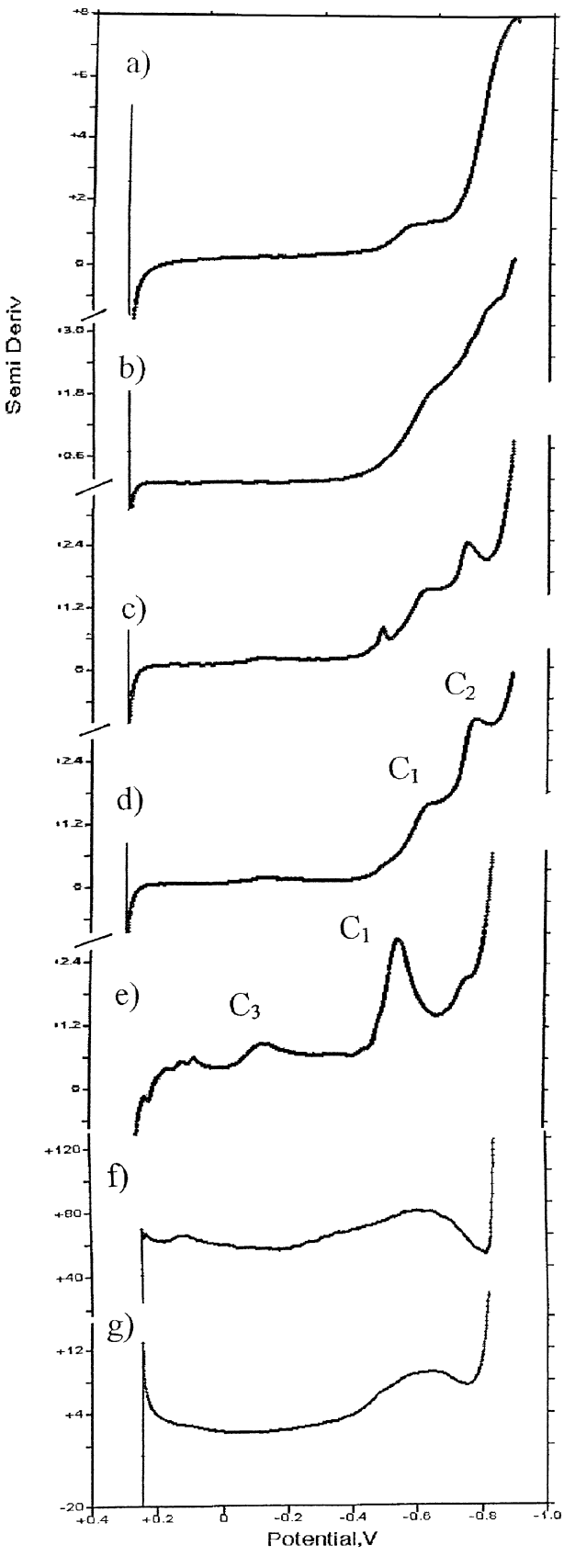

Fig. 2 Cathodic LSVs after semi-derivative convolution of PIGEs modified by (**a**) Co(II) spinel, (**b**) cordierite glass, (**c**) μ-cordierite, (**d**) α-cordierite, (**e**) β-cordierite and (**f**) CoO. Electrolyte: 0.10 M HCl plus 0.90 M NaCl. Curve (**g**) corresponds to an unmodified PIGE immersed in 1.0 mM $Co(NO_3)_2.6H_2O$ in the same electrolyte medium. Potential scan initiated at +0.85 V in the negative direction. Potential scan rate: 20 mV/s

(vide infra), the anodic processes at more positive potentials may consist of the oxidation of Co(II) chloride complexes to Co(III) ones in the solution phase:

$$CoCl_x^{(2-x)+} + (y-x)Cl^- \rightarrow CoCl_y^{(3-y)+} + e^- \quad (3)$$

For powdered Co attached to PIGEs, an oxidative dissolution to Co(III) chloride complexes appears to be operative:

$$Co(s) + yCl^- \rightarrow CoCl_y^{(3-y)+} + 3e^- \quad (4)$$

It should be noted that, although the standard electrode potential for the Co^{3+}/Co^{2+} couple is very high (ca. +1.6 V vs. SCE), complex formation can stabilize significantly the Co(III) oxidation state. Thus, CoO can be oxidized following a scheme similar to that described by Grygar [37] for chromium oxide as:

$$CoO(s) + 2H^+ + yCl^- \rightarrow CoCl_y^{(3-y)+} + H_2O + e^- \quad (5)$$

Eventually, a solid-to-solid transformation such as:

$$CoO(s) + H_2O \rightarrow CoO(OH)(s) + H^+ + e^- \quad (6)$$

can occur. In subsequent cathodic scans, solid Co(III) forms can undergo reductive dissolution processes or solid state processes, yielding Co(II) materials:

$$CoO(OH)(s) + H^+ + e^- \rightarrow CoO(s) + H_2O \quad (7)$$

Solid state processes may involve, however, quite different mechanisms, depending on the structure of the solid and the pH. Thus, the electrochemical reduction of $LiCoO_2$ in alkaline electrolytes may involve proton insertion/deintercalation [24], while in strong NaOH electrolytes it has been described in terms of a complex intercalation mechanism with participation of hydrated Na^+ ions and gradual expansion of the host interlayer spacing [25].

Electrochemistry of cordierite materials

Figure 2 shows the cathodic LSVs for $Co(NO_3)_2.6H_2O$ in 0.10 M HCl + 0.90 M NaCl solution and the studied cobalt materials after applying a semi-derivative convolution to improve peak resolution. As can be seen in Fig. 2a, well-defined cathodic peaks at −0.43 V and −0.84 V appear for Co(II) spinel. For cordierite glass (Fig. 2b), two ill-defined overlapped peaks at −0.52 (C_1) and −0.76 V (C_2) are recorded, while for crystalline cordierite specimens, well-defined signals appear, with

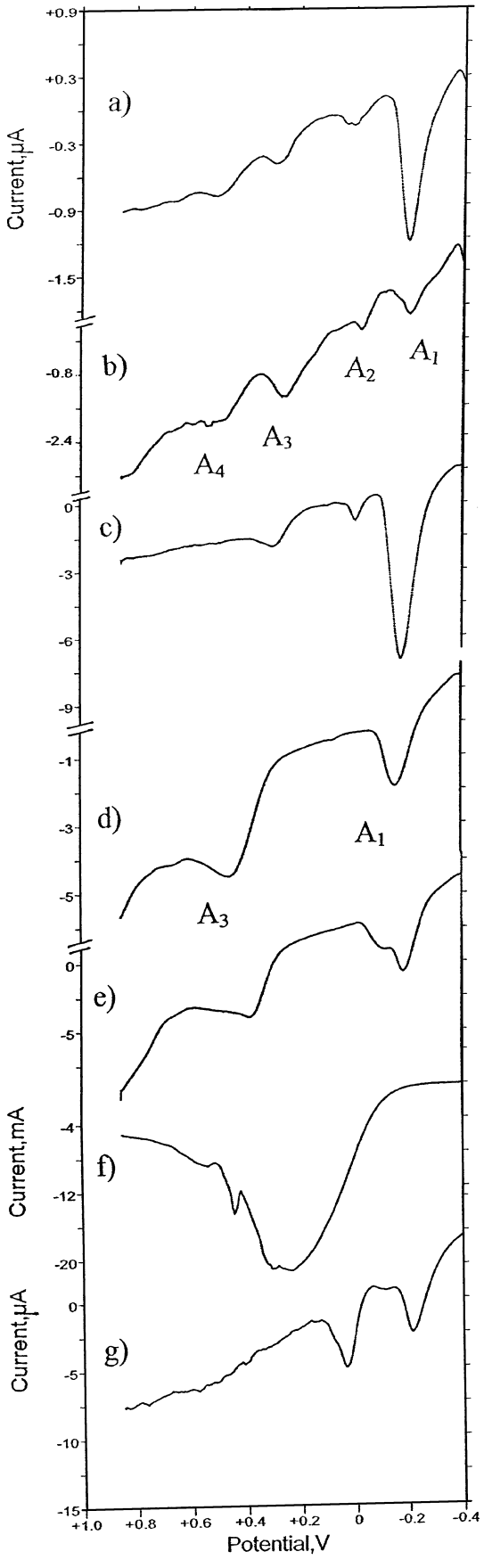

Fig. 3 Anodic LSVs for (**a**) cordierite glass, (**b**) μ-cordierite, (**c**) α-cordierite, (**d**) β-cordierite, (**e**) CoO and (**f**) Co attached to PIGEs. Electrolyte: 0.10 M HCl plus 0.90 M NaCl. Curve (**g**) corresponds to an unmodified PIGE immersed in 1.0 mM $Co(NO_3)_2.6H_2O$ in the same electrolyte medium. Potential scan initiated at −0.85 V in the positive direction. Potential scan rate: 20 mV/s

cathodic peaks at −0.47 V and −0.66 V for μ-cordierite (Fig. 2c), at +0.22, −0.48 and −0.68 V for α-cordierite (Fig. 2d), and at +0.28 (C_3), −0.38 (C_1) and −0.65 V (C_2) for β-cordierite (Fig. 2e). For CoO (Fig. 2f), an ill-defined wave appears near to −0.65 V, similar to that recorded for a 1.0 mM solution of $Co(NO_3)_2.6H_2O$ (Fig. 2g). For Co powder attached to a PIGE, as expected, no reduction waves were detected.

Anodic scan LSVs also revealed significant differences among the studied cordierites, as illustrated in Fig. 3. Upon initiating the potential scan at −0.85 V, a tall peak near to −0.18 V (A_1) appeared in all cases, followed by anodic peaks at +0.05 (A_2), +0.28 (A_3) and +0.52 V (A_4) for cordierite glass (Fig. 3a) and μ-cordierite (Fig. 3b), whereas for α- and β-cordierite (Fig. 3c and Fig. 3d, respectively) only one well-defined anodic peak near to +0.40 V (A_3) accompanied the stripping process at −0.18 V (A_1). This behaviour is similar to that displayed by CoO (Fig. 3e), for which an anodic wave near to +0.75 V follows the peaks at −0.18 V and +0.40 V. For powdered Co attached to PIGEs, a prominent stripping peak appears near to +0.25 V, as illustrated in Fig. 3f, whereas the stripping peak A_1 is absent. This suggests that the response of cobalt grains can be described by Eq. 5, while the oxidation of Co metal electrochemically deposited from cordierites mainly proceeds via Eq. 2. In voltammograms of $Co(NO_3)_2.6H_2O$ in solution (see Fig. 3g), however, both stripping anodic peaks A_1 and A_5 appear, suggesting that Eqs. 2 and 4 apply.

This is in principle consistent with literature data; thus, remarkable differences in the stripping of abrasively deposited and electrochemically deposited lead have been reported by Lovric et al. [38].

This electrochemistry remains essentially unchanged by varying the electrolyte media from 1.0 M HCl to 0.01 M HCl + 0.99 M NaCl. The unique electrode process that experiences significant peak potential changes is the reduction process near to +0.25 V (C_3) recorded for crystalline cordierites, which is shifted toward more positive values on decreasing the pH.

The voltammetric response recorded for the studied materials in 0.10–1.0 M NaCl media was quite similar to that described in acidic media. As shown in Fig. 4, cathodic LSVs of cobalt spinel (Fig. 4a) present a prominent reduction at −0.40 V accompanied by a wave at −0.85 V. The response of cordierite glass (Fig. 4b) consists of two prominent overlapped peaks at −0.53 V and −0.66 V, preceded by a tall peak at −0.18 V. The response of crystalline cordierites μ, α and β (Fig. 4c, Fig. 4d and Fig. 4e, respectively) is similar, with peaks at −0.42 V and −0.62 V and an additional reduction

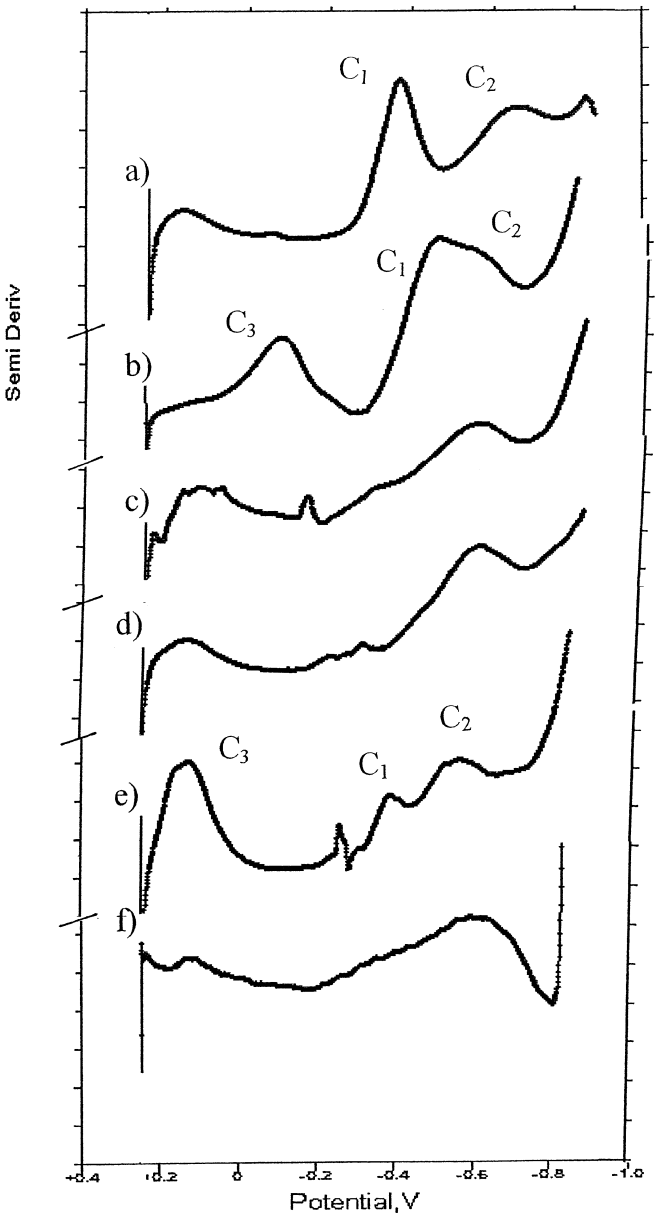

Fig. 4 Cathodic LSVs after semi-derivative convolution of PIGEs modified by (**b**) Co(II) spinel, (**b**) cordierite glass, (**c**) μ-cordierite, (**d**) α-cordierite, (**e**) β-cordierite and (**f**) CoO. Electrolyte: 1.0 M NaCl. Potential scan initiated at +0.25 V in the negative direction. Potential scan rate: 20 mV/s

peak at +0.18 V. This peak also appears in PIGEs modified by CoO (see Fig. 4f), preceding a broad peak at −0.65 V. Anodic LSVs were similar for all cordierite samples, with a stripping oxidation process near to −0.25 V followed by peaks at +0.10 V and +0.30 V. The response of cobalt spinel is similar, while that of CoO consisted essentially of an ill-defined but intense oxidation wave near to +0.5 V. The pertinent peak potential data are summarized in Table 1.

The net amount of charge passed in the reduction of cobalt cordierites can be estimated by determining the area under the voltammetric curve. Using the stripping peak at −0.18 V, charges of 10 μC were obtained for cordierites after transference of 0.15 mg of the solid material to the PIGE. These values provide a similar relationship between the number of electroactive Co^{2+} centres and their total number, consistently equal of that obtained for CoO and cobalt spinel (1.2×10^{-4}), as shown in Table 2. This result suggests that similar reaction schemes are operative for CoO, cobalt spinel and cobalt cordierites.

Accordingly, in view of the presence of well-developed stripping peaks (A_1) corresponding to the oxidation of cobalt metal, reduction of cordierites in the −0.2 to −0.7 V potential range can tentatively be represented as:

$$Co_2Al_4Si_5O_{18}(s) + 6H^+ + 4e^- \rightarrow 2Co(s) + 5SiO_3^{2-} + 4Al^{3+} + 3H_2O \quad (8)$$

The presence of two well-separated cathodic peaks C_1 and C_2 in the cordierites can be explained in terms of (1) the existence of a significant heterogeneity in the shape and size distribution of the cordierite particles, (2) the coexistence of different electrochemical pathways for the reduction of Co^{2+} centres, and (3) the coexistence of Co^{2+} centres with different coordinative arrangements. The last possibility appears to be supported by the recognized variation of the degree of disorder in the lattice from low- to high-temperature cordierites [5, 6].

For the cordierites, peaks C_2 and A_3 behave as expected for irreversible reductive dissolution or oxidative dissolution processes [37], the peak potential varying linearly with the logarithm of the potential scan rate. The peak potentials of C_1 and C_3, however, remain essentially scan-rate independent in the range from 5 to 500 mV/s, suggesting that different electrochemical mechanisms are involved. This is consistent with the observation of a weak stripping peak (A_2) at potentials slightly more positive than those of A_1, suggesting that two electrochemically distinct deposits of cobalt metal are formed.

The oxidation processes involving cordierite materials near to +0.3 V (A_3) can correspond to an oxidative dissolution process:

$$Co_2Al_4Si_5O_{18}(s) + 6H^+ + 2yCl^- \rightarrow 2CoCl_y^{(3-y)+} + 5SiO_3^{2-} + 4Al^{3+} + 3H_2O + 2e^- \quad (9)$$

whereas the anodic process at more positive potentials (A_4) for cobalt cordierite glass and μ-cordierite probably results in the formation of solid Co(III) forms. These should be subsequently reduced in cathodic scan voltammograms in the electrode process C_3.

Correlation between electrochemical and structural data

The electrochemical response of cobalt cordierite specimens and reference materials can be interpreted in terms of the influence of (1) the microstructural environment of cobalt centres, namely tetrahedral for cobalt spinel

Table 1 Selected peak potential data for electrode processes involving cobalt materials attached to PIGEs. From LSVs at 20 mV/s

Electrolyte	HCl			NaCl			NaOH	
Peak/E_p (mV)	C_3	C_1	C_2	C_3	C_1	C_2	C_1	C_2
Cobalt spinel	–	−430	−840	–	−405	−850	–	–
Cordierite glass	–	−515	−760	−175	−530	−665	−455	−530
μ-Cordierite	+250	−470	−655	−160	−375	−630	−450	−550
α-Cordierite	+220	−485	−685	–	−430	−645	−455	−550
β-Cordierite	–	−440	–	–	−420	−600	−440	−550
CoO	–	–	−720	–	–	−720	–	−560

Electrolyte	HCl		NaCl		NaOH	
Peak/E_p(mV)	A_4	A_3	A_4	A_3	A_4	A_3
Cobalt spinel	–	+330	–	+305	–	–
Cordierite glass	+700	+325	+605	+320	–	+360
μ-Cordierite	+650	+360	–	+255	–	+360
α-Cordierite	+605	+355	–	+305	–	+370
β-Cordierite	+600	+320	+600	+245	–	+380
CoO	+750	–	+680	–	+620	+240

Table 2 Charge passed (Q) in process A_1, total number of cobalt centres (n_{Co}) and number of electroactive cobalt centres (n_{Co}*) in the studied materials. From LSVs in 0.10 M HCl + 0.90 M NaCl. Transference of 1.5 mg of modifier on electrodes. Geometrical area 0.78 cm^2. Potential scan rate 20 mV/s. Electrocatalytic effect of PIGEs modified by different cobalt materials in 2.0 mM mannitol + 0.10 M NaOH. Peak current (i_p) in LSVs at 20 mV/s. In all cases, mean data from three independent measurements. Numbers in parentheses denote the uncertainty in the last significant figure

Material	Q (μC)	n_{Co} (mol)	n_{Co}* (mol)	n_{Co}*/n_{Co}	i_p (μA)	i/n_{Co} (A/mol)
Cordierite glass	10(1)	$4.6(5)\times10^{-7}$	$5.2(5)\times10^{-11}$	$1.1(2)\times10^{-4}$	1400(40)	$3.0(3)\times10^{3}$
μ-Cordierite	11(1)	$4.6(5)\times10^{-7}$	$5.7(6)\times10^{-11}$	$1.2(2)\times10^{-4}$	3100(5)	$6.7(7)\times10^{3}$
α-Cordierite	11(1)	$4.6(5)\times10^{-7}$	$5.7(6)\times10^{-11}$	$1.2(2)\times10^{-4}$	4200(50)	$9.1(8)\times10^{3}$
β-Cordierite	10(1)	$4.6(5)\times10^{-7}$	$5.2(5)\times10^{-11}$	$1.1(2)\times10^{-4}$	2800(40)	$6.1(6)\times10^{3}$
Cobalt spinel	23(2)	$8.5(8)\times10^{-7}$	$1.1(1)\times10^{-10}$	$1.4(3)\times10^{-4}$	160(5)	$1.9(2)\times10^{2}$
CoO	42(3)	$2.0(2)\times10^{-6}$	$2.2(2)\times10^{-10}$	$1.1(2)\times10^{-4}$	3000(50)	$1.5(2)\times10^{3}$

and (partly) in cordierite glass and octahedral for CoO and crystalline cordierites; (2) the mesostructural environment, consisting of more or less disordered subsystems of layers of hexagonal rings connecting through M^{2+} octahedra and T_1 tetrahedra [5, 6].

Thus, for cordierite glass an ill-defined response arising from the superposition of the responses of tetrahedral and octahedral Co^{2+} ions appears. The cathodic voltammetric profile (see Figs. 2 and 4) looks like a combination of voltammetric curves for cobalt spinel and crystalline cordierites. In the series μ-, α- and β-cordierite, two separated peaks C_1 and C_2 appear, indicating that probably two electrochemical pathways coexist. For β-cordierite the peak C_1 prevails largely, suggesting that this electrode process is associated with ordered mesostructures, while the peak C_2 would correspond to disordered ones.

These considerations, however, must take into account the peculiar nature of the reductive processes of solids. Such processes occur essentially at the boundary of at least three different phases: the solid substrate electrode, the solid sample, and the electrolyte solution [16, 23]. The overall reaction rate can be controlled by electron transfer from the substrate electrode to the reactant phase, the electron transfer from the product phase to the reactant phase, reactions of complexation and/or proton insertion, and the diffusion of ions into the solution. When a new solid phase is formed, nucleation and growth processes involving the new phase may appear as the rate-determining steps.

In the case of the reduction of cobalt(II) materials, the overall electrochemical mechanism may involve a solid state interconversion, as obtained for lead oxide [16], or a dissolution/crystallization scheme operative for lead hydroxychloride [16].

Since the studied electrode processes are essentially pH independent, it appears that the rate-determining step may be associated with the mechanism of electron transfer and/or lattice destruction/reconstruction rather than proton insertion or complexation reactions in the solution phase. It is well known that the inverse process, the electrochemical formation of solid deposits from species in solution, can occur through different mechanisms of nucleation and growth [39, 40, 41, 42]. Conversely, one can expect that, under determined circumstances, the dissolution of a solid can be strongly conditioned by the mechanisms of lattice destruction/formation.

The mechanisms of nucleation (instantaneous, progressive) and growth (with or without diffusive control, cylindrical, hemispherical, etc.) can be discerned through different current–time dependencies of $i \propto t^x$ in chronoamperometric experiments. This scheme was applied to current–potential curves in the diffusive region of the

voltammetric peaks C_1 and C_2. Following the literature [43, 44, 45, 46] for "ordinary" diffusion-controlled electron transfer processes in the solution phase, at potentials sufficiently "behind" the voltammetric peak the current obeys the Cottrell equation, i.e. $i \propto t^{-1/2}$, and, accordingly, a linear relationship between i^{-2} and the applied potential, E, holds. Following this line of reasoning, in the region of voltammograms dominated by the kinetics of the deposition/dissolution process, linear dependences between $i^{1/x}$ and E must be operative. Interestingly, peak C_1 provides a linear relationship between $i^{1/2}$ and $E-E_p$, suggesting that a rate law $i \propto t^2$ is operative. This corresponds to a mechanism of progressive nucleation in two dimensions [39]. For peak C_2, however, the best linearity was found between $i^{2/3}$ and $E-E_p$, for which there is no definite model. These results are in agreement with the idea that different reductive mechanisms are responsible for peaks C_1, associated with ordered crystalline mesostructures, and C_2, associated with disordered mesostructures.

In view of the recognized possibility of forming solid solutions with exchange of Co^{2+} ions by Mg^{2+} ones, a complementary series of experiments was performed in $HCl + MgCl_2$ electrolytes. The cathodic and anodic LSVs for β-cordierite in 0.50 M $MgCl_2$ are shown in Fig. 5. The most relevant aspect is the increase of the cathodic peak at −0.60 V at the expense of that recorded at −0.40 V in NaCl electrolytes and the appearance of a reduction process near to −0.15 V (see Fig. 5a). In anodic scan LSVs (see Fig. 5b), the peak A_3 is slightly displaced toward more negative potentials, while there appears a subsequent oxidation peak (A_4) at more positive potentials.

These data can be rationalized by taking into account the dynamic nature of the reductive/oxidative dissolution processes. At a nanoscopic scale, lattice construction and lattice destruction occur, the equilibrium being reached when the dissolution rate equals the crystallization rate. Consistent with the foregoing set of considerations, the presence of Mg^{2+} ions able to substitute Co^{2+} ones in the cordierite lattice results in the formation of "disordered" mesostructures through a dissolution/substitution/lattice reconstruction mechanism which can tentatively be represented by the equation:

$$Co_2Al_4Si_5O_{18}(s) + xMg^{2+} + 2xe^- \rightarrow xCo(s) + Co_{2-x}Mg_xAl_4Si_5O_{18}(s) \quad (10)$$

The formation of mixed "disordered" Co/Mg-substituted cordierite results in the increase of peak C_2 at the expense of peak C_1. A similar reasoning can be applied for the oxidative processes:

$$Co_2Al_4Si_5O_{18}(s) + xMg^{2+} \rightarrow xCo^{3+} + Co_{2-x}Mg_xAl_4Si_5O_{18}(s) + xe^- \quad (11)$$

Then, the reduction and oxidation of mixed $Co_{2-x}Mg_xAl_4Si_5O_{18}$ should take place at electrode potentials different from those of non-substituted

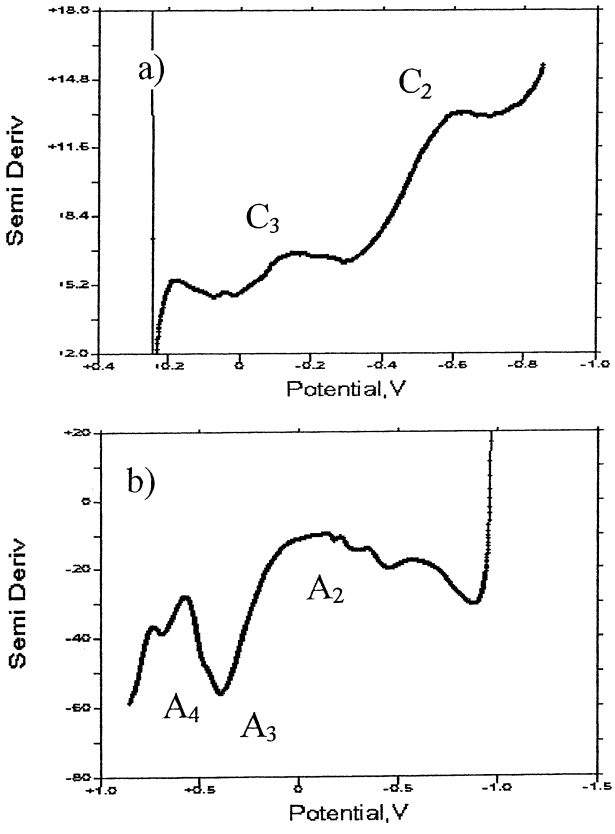

Fig. 5 LSVs of β-cordierite immersed in 0.50 M $MgCl_2$: (**a**) potential scan initiated at +0.25 V in the negative direction; (**b**) potential scan initiated at −1.05 V in the positive direction. Potential scan rate: 20 mV/s

$Co_2Al_4Si_5O_{18}$ ones. Consistent with that scheme, the voltammetry of cobalt cordierites in $MgCl_2$ increasingly differ from that in NaCl on decreasing the potential scan rate.

In this context, formation of solid Co(III) materials (electrochemical process A_4) appears to be disfavoured by the existence of exigent structural constraints. This is illustrated by LSVs in Fig. 3: peak A_4 appears well defined for cordierite glass and μ-cordierite, but disappears for α- and β-cordierites. In fact, the region of potentials in which peak A_4 appears exhibits tall peaks for cordierite glass in experiments performed by pressing the graphite electrode against a spot of powdered material deposited on a glass tile. This electrode conditioning results in the transference of lead oxide that is reduced to lead metal at potentials close to −0.55 V. Then, lead is deposited in anodic scan LSVs, as demonstrated by the appearance of a stripping peak at −0.48 V (A_5) in the voltammograms (see Fig. 6a). Apart from this peak, this procedure does not produce any significant modification in the LSVs of α- and β-cordierite (Fig. 6b). For cordierite glass and μ-cordierite, however, a lot of tall anodic peaks are recorded in the +0.15 V to +0.80 V potential range, labelled as A_6, A_3 and A_4 in Fig. 6a. Apparently, deposition of lead metal eases electron transfer processes of solid microparticles.

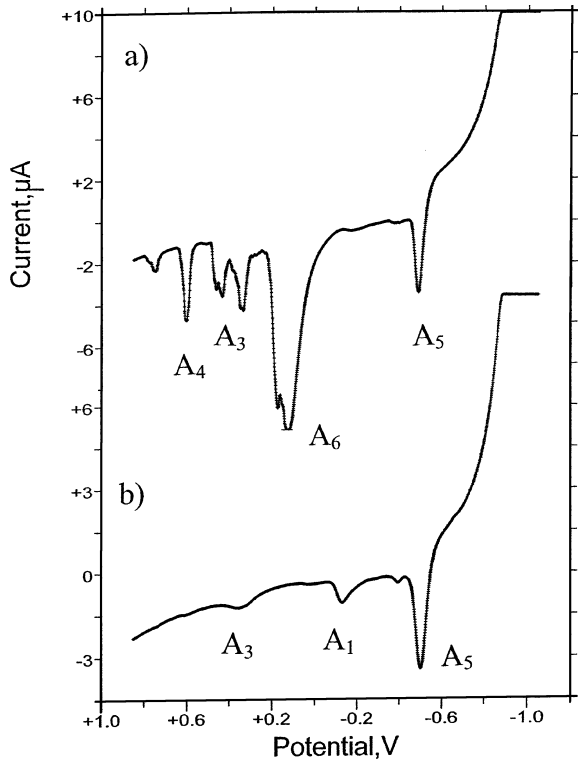

Fig. 6 Anodic LSVs of (**a**) cobalt cordierite glass and (**b**) α-cordierite transferred to PIGEs over a PbO-rich glass surface. Potential scan initiated at −1.05 V in the positive direction without prior electrogeneration step. Potential scan rate: 20 mV/s

For our purposes, the relevant point to emphasize is that glass or disordered structures rather than ordered ones permit the electrochemical formation of solid Co(III) species.

Electrocatalytic effect on the oxidation of mannitol

In order to assess the possibility of structure/electrochemistry correlations, the catalytic effect exerted by cobalt materials on the electrochemical oxidation of mannitol in alkaline media was studied.

Preliminary experiments performed upon immersion of sample-modified electrodes in NaOH + NaCl electrolytes produced voltammetric responses with a main reduction peak near to −0.45 V (C_1) overlapped by a second one at −0.55 V (C_2), as depicted in Fig. 7a–c, similar to that obtained for CoO (see Fig. 7d). This response is quite similar to that obtained in acidic and neutral electrolytes. Consistently, in the anodic region a well-defined oxidation peak was obtained for all cordierite samples near to +0.38 V (A_3), with a profile similar to that obtained in neutral media.

Figure 8 illustrates the typical behaviour of cordierite-modified PIGEs with regard to the electrochemical oxidation of mannitol in alkaline media. After background subtraction, LSVs of cobalt cordierites in 2.0 mM mannitol + 0.10 M NaOH solutions exhibit a

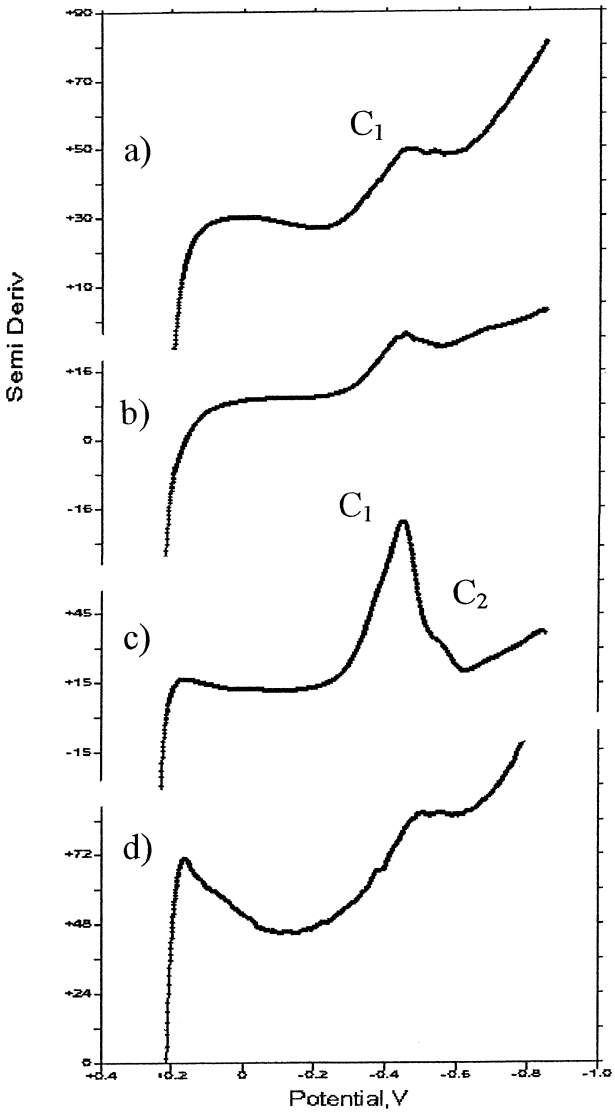

Fig. 7 Cathodic LSVs after semi-derivative convolution of PIGEs modified by (**a**) cordierite glass, (**b**) α-cordierite, (**c**) β-cordierite and (**d**) CoO. Electrolyte: 0.10 M NaOH. Potential scan initiated at +0.25 V in the negative direction. Potential scan rate: 20 mV/s

prominent anodic peak at +1.04 V, denoting the existence of an intense electrocatalytic effect.

This electrocatalytic effect is prompted by the vicinity of the potential of the Co(III)/Co(II) couple to that of mannitol oxidation, a condition for mediated electrocatalysis [30, 46]. Since the electrode oxidation of alcohol groups takes place at potentials more positive than those where Co(III) species are generated, it appears reasonable to conjecture that the rate-determining step consists of a reaction between the electrochemically generated Co(III) and the substrate RCH_2OH, followed by electrode oxidation of the generated radical intermediates.

These can be represented as:

$$Co(II) \rightarrow Co(III) + e^- \qquad (12)$$

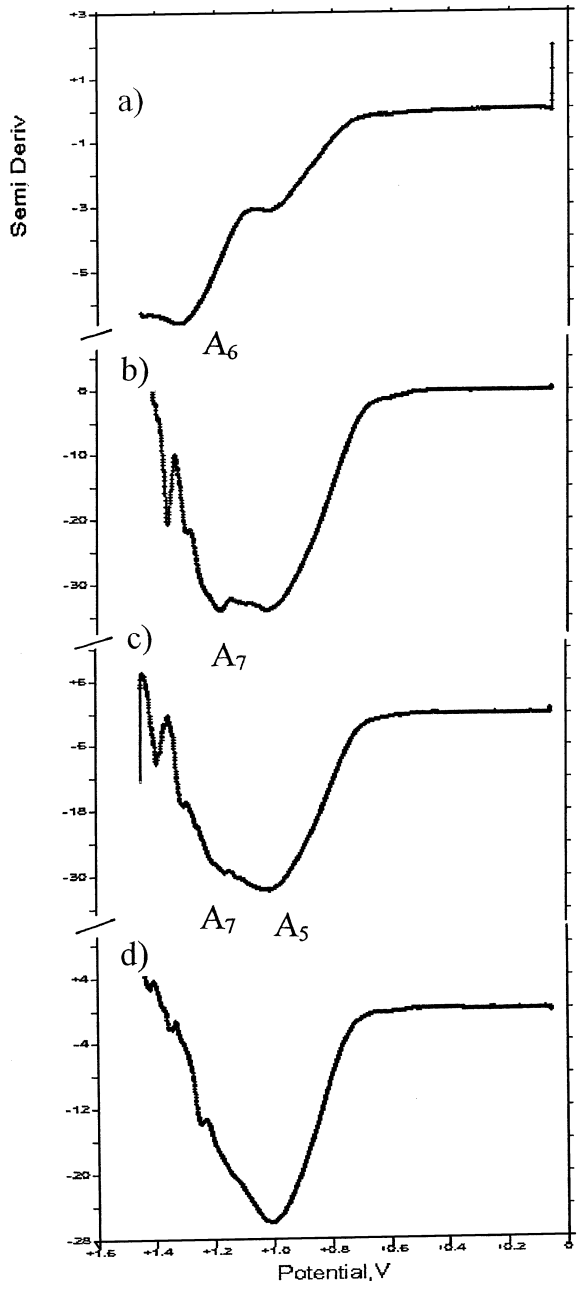

Fig. 8 Anodic LSVs after semi-derivative convolution of PIGEs modified by (**a**) cordierite glass, (**b**) μ-cordiertie, (**c**) α-cordierite and (**d**) β-cordierite immersed in 2.0 mM mannitol + 0.10 M NaOH. Potential scan initiated at +0.05 V in the positive direction. Potential scan rate: 20 mV/s

$$\mathrm{Co(III)} + x\mathrm{RCH_2OH} \rightarrow \mathrm{Co(II)} + x\mathrm{OH^-} + x\mathrm{R\dot{C}HOH} \quad (13)$$

$$\mathrm{R\dot{C}HOH} \rightarrow \mathrm{Products} + \mathrm{e^-} \quad (14)$$

as described for the catalysis of the oxidation of sugars and alditols by cobalt oxide-based glassy carbon electrodes [30, 36].

For our purposes, it should be emphasized that the studied materials exhibit significant differences with regard to their catalytic effect on mannitol oxidation as depicted in Figs. 1, 2, 3, 4. Interestingly, for cordierite glass, two well-defined peaks appear at +1.04 V (A_5) and +1.35 V (A_6), in agreement with the existence of two different cobalt sites. For crystalline cordierites they look like two superimposed peaks at +1.04 V (A_5) and +1.20 V (A_7), the first being enhanced at the expense of the second along the series μ-, α-, β-cordierite. This response can be explained in agreement with prior considerations on attributing the catalytic processes A_5 and A_7 to "ordered" and disordered cordierite mesostructures with octahedrally coordinated cobalt centres. The catalytic process A_6 must be associated with tetrahedral cobalt centres almost exclusively composed of cordierite glass.

The total peak height varies significantly from one material to another, growing in the order cordierite glass < μ-cordierite < β-cordierite < α-cordierite, the observed peak currents ranging from 1400 μA to 4200 μA in LSVs at 20 mV/s in 2.0 mM mannitol + 0.10 M NaOH. It is interesting to note that cobalt cordierites display an electrocatalytic effect toward mannitol oxidation per cobalt center that is 2–5 times larger than those of cobalt oxide and 15–45 times larger than cobalt spinel. The corresponding data are shown in Table 2.

Conclusions

The voltammetry of cobalt cordierites, cobalt oxide and cobalt spinel attached to PIGEs can be described in terms of the reduction of Co(II) materials to cobalt metal and their oxidative dissolution superimposed with the formation of Co(III) solid phases.

The reduction of cordierites occurs via two voltammetric processes at potentials close to −0.40 V and −0.65 V. Two different electrochemical pathways are operative for the reduction of pristine materials, involving different modes of lattice destruction/construction.

Such electrode processes reflect the differences in the microenvironment of cobalt centres (tetrahedral and octahedral coordination) and the mesostructural arrangement of the material, resulting in more or less ordered/disordered distribution of aluminum-containing tetrahedra.

Solid state oxidation of Co(II) forms to Co(III) appears to be associated with the existence of weak structural demands in cordierite glass and μ-cordierite. Such processes are absent in α- and β-cordierite.

Cobalt cordierites exhibit a significant catalytic effect on the reduction of mannitol in aqueous alkaline media. Differences in microstructural and mesostructural arrangements result in the appearance of different oxidation peaks at +1.04 V and +1.20 V, associated with ordered and disordered mesostructures with octahedrally coordinated cobalt in μ-, α- and β-cordierite, +1.20 V, and at +1.35 V, associated with tetrahedrally coordinated cobalt in cordierite glass.

Although further research is needed to clarify the detailed mechanisms involved in the electrochemistry of cordierites and their catalytic ability on mannitol oxidation, these results provide a reasonable support to the idea that definite correlations between micro/mesostructure arrangement and electrochemistry can be obtained from the voltammetry of microparticles approach.

Acknowledgements We thank the Valencian Regional Government, project CTIDIB/2002/216, for financial support.

References

1. Watanabe K, Giess EA (1985) J Am Ceram Soc 68:C102
2. Watanabe K, Giess EA, Shafer MW (1985) J Mater Sci 20:508
3. Karkhanavala MD, Hummel FA (1953) J Am Ceram Soc 36:389
4. Gibbs GV (1966) Am Mineral 51:1068
5. Meagher EP, Gibbs GV (1977) Can Mineral 15:43
6. Putnis A (1980) Contrib Mineral Petrol 74:135
7. Goldman DS, Rossman GR, Dollase WA (1977) Am Mineral 62:1144
8. Selkregg KR, Bloss FD (1980) Am Mineral 65:522
9. Ikawa H, Otagiri T, Imal O, Suzuki M, Urabe K, Udagawa S (1986) J Am Ceram Soc 69:492
10. Sundar S, Vepa VSS, Umarji AM (1993) J Am Ceram Soc 76:1873
11. Chen YF, Rabu P, Pourroy G, Vilminot S (1995) Eur J Solid State Inorg Chem 32:1065
12. Wandscheneider P, Seifert F (1984) J Am Ceram Soc 67:C163
13. Sales M, Alarcón J (1995) J Mater Sci 30:2341
14. Villegas MA, Alarcón J (2002) J Eur Ceram Soc 22:487
15. Torres FJ, Alarcón J (2003) J Eur Ceram Soc (in press)
16. Scholz F, Meyer B (1998) In: Bard AJ. Rubinstein I (eds) Electroanalytical chemistry, a series of advances, vol. 20. Dekker, New York, pp 1–87
17. Lamache M, Bauer D (1979) Anal Chem 51:1320
18. Brainina KhZ, Vidrevich MB (1981) J Electroanal Chem 121:1
19. Scholz F, Nitschke L, Henrion G (1989) Naturwissenschaften 76:71
20. Scholz F, Nitschke L, Henrion G, Damaschun F (1989) Naturwissenschaften 76:167
21. Scholz F, Lange B (1992) Trends Anal Chem 11:359
22. Scholz F Meyer B (1994) Chem Soc Rev 23:341
23. Grygar T, Marken F, Schröder U, Scholz F (2002) Collect Czech Chem Commun 67:163
24. Rao MM, Liebenow C, Jayalakshami M, Wulff H, Guth U, Scholz F (2001) J Solid State Electrochem 5:348
25. Frangini S, Carewska M, Passerini S, Scaccia S (2001) J New Mater Electrochem Syst 4:83
26. Rao MM, Jayalakshmi M, Schäf O, Wulff H, Scholz F (2001) J Solid State Electrochem 5:50
27. Cox JA, Jaworski RK, Kulesza PJ (1991) Electroanalysis 3:969
28. Ghosh PK, Bard AJ (1983) J Am Chem Soc 105:5691
29. Rolison DR, Nowak RJ, Welsh TA, Murray CG (1991) Talanta 38:27
30. Casella IG, Cataldi TRI, Salvi AM, Desimoni E (1993) Anal Chem 65:3143
31. Doménech A, Alarcón J (2002) Anal Chim Acta 452:11
32. Luo P, Prabhu SV, Baldwin RP (1990) Anal Chem 62:752
33. Wang J, Taha Z (1990) Anal Chem 62:1413
34. Jadeii JM, Marioli J, Kuwana T (1991) Anal Chem 63:649
35. Xie Y, Huber CO (1991) Anal Chem 63:1714
36. Cataldi TRI, Guerrieri A, Casella IG, Desimoni E (1995) Electroanalysis 7:305
37. Grygar T (1996) J Electroanal Chem 405:117
38. Lovric M, Komorsky-Lovric S, Bond AM (1991) J Electroanal Chem 319:1
39. Schultze JW, Lohrengel MM (1983) Electrochim Acta 28:973
40. Gunawardena G, Hills G, Montenegro I (1985) J Electroanal Chem 184:357
41. de Levie R (1988) Chem Rev 88:599
42. Crousier J, Bimaghra I (1989) Electrochim Acta 34:1205
43. Nicholson RS (1965) Anal Chem 37:667
44. Polcyn DS, Shain I (1966) Anal Chem 38:370
45. Bontempelli G, Magno, F, Daniele S (1985) Anal Chem 57:1503
46. Andrieux CP, Dumas-Bouchiat JM, Saveant JM (1982) J Electroanal Chem 131:1